Journal of Electronics and Information Science (2026)
Clausius Scientific Press, Canada

DOI: 10.23977/jeis.2026.110101
ISSN 2371-9524 Vol. 11 Num. 1

High-Precision Digital Temperature Control Method for Rubidium Atomic Clocks

Wang Xin, Li Shiguang, Chen Zhigao

Beijing Institute of Radio Metrology and Measurement, Beijing, China

Keywords: Rubidium Atomic Clock; Digital Temperature Control; Second-Order System; PI Control

Abstract: Rubidium atomic clocks' frequency stability and accuracy are highly sensitive to lamp and cavity temperature fluctuations. To address limitations of conventional analog control and digital PID control, this study proposes a high-precision digital temperature control method based on second-order system modeling and PI control. Equivalent models are established, parameters are quantitatively determined via heater gain calibration, and an integral limiting strategy is adopted. Experiments show steady-state temperature fluctuations of ±0.04 ℃ (lamp) and ±0.02 ℃ (cavity), enabling fast, accurate, and stable regulation without empirical tuning, improving clock performance and providing a reliable solution for precision temperature control.

1. Introduction

Rubidium atomic clocks, as key time and frequency references, are widely used in communication, navigation, aerospace, and high-precision metrology, with their long-term frequency stability and accuracy being critical to system performance[1]. In their physical systems, lamp and resonant cavity temperature fluctuations significantly affect atomic transitions, altering excitation efficiency and cavity resonant frequency, thus causing output frequency deviations[2]. A 1 ℃ cavity temperature change can induce a frequency accuracy variation of ~3×10^{-10}, making high-precision, fast, and stable control of these two temperatures a key technology and urgent engineering challenge for improving clock performance[3].

Current temperature control in rubidium atomic clocks mainly relies on conventional analog control and digital PID control. Analog schemes use temperature bridges with analog PI/PID circuits for closed-loop control, featuring simple structures and good real-time performance but fixed hardware-determined setpoints and poor stability/universality due to component drift and environmental interference[4]. Digital PID control, leveraging analog-to-digital conversion and digital algorithms, enables adjustable setpoints[5], but its parameter tuning is experience-dependent, and the derivative term amplifies noise and high-frequency disturbances, leading to control signal fluctuations or oscillations[6]. It thus struggles to balance high stability and fast response in high-precision scenarios, with limitations in dynamic range and parameter consistency.

To address these issues, this paper proposes a high-precision digital temperature control method based on second-order system modeling and PI control[7]. Lamp and cavity temperature control loops are equivalently modeled as second-order thermal inertia systems, with proportional and

integral parameters quantitatively determined via heater gain calibration, eliminating empirical tuning[8]. An integral limiting strategy is introduced to prevent control signal saturation, enhance stability, and avoid derivative term-induced noise amplification. The method balances response speed and stability, ensures high control accuracy, and enables flexible software-adjustable setpoints to optimize clock operating temperatures.

2. High-Precision Digital Temperature Control Method Based on PI Control

2.1 Overall Architecture of the Temperature Control System

The digital temperature control system designed in this study adopts a microcontroller as the core control unit and consists of four main modules, as shown in Figure.1.

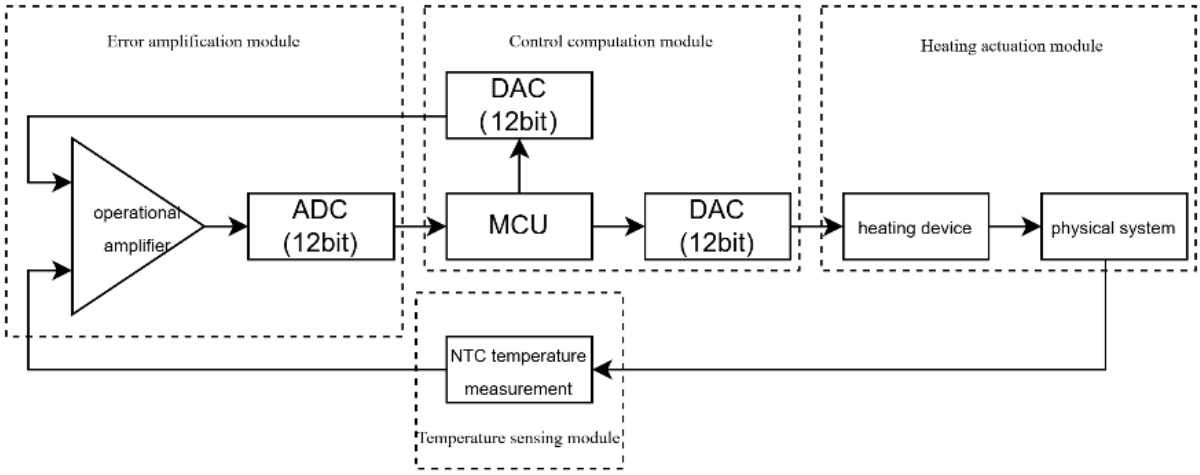

Figure.1 Block diagram of digital temperature control system

(1) Temperature sensing module: A high-precision NTC thermistor measures the real-time temperatures of the lamp and resonant cavity, with its temperature-dependent resistance converted into a proportional voltage signal via a voltage divider circuit for accurate measurement.

(2) Error amplification module: An operational amplifier differentially amplifies the deviation between the target temperature reference voltage and the measured temperature voltage, with the gain designed based on the temperature sensing range and ADC input range to ensure sufficient resolution.

(3) Control computation module: The microcontroller acquires the amplified error signal through an ADC, computes the heating control signal via a PI algorithm, and adopts an integral limiting strategy to avoid integral windup and improve stability.

(4) Heating actuation module: A DAC converts the digital control signal into an analog voltage to drive the heating element, realizing precise and reliable temperature regulation of the lamp and resonant cavity.

2.2 Modeling of the Temperature Control System

Conventional digital temperature control systems usually adopt PID control, where the derivative term enhances dynamic response by predicting error signal trends based on its rate of change[9]. However, in rubidium atomic clock temperature control, the derivative term has notable drawbacks: Noise sensitivity; Limited effect due to system inertia; Increased parameter tuning complexity. Thus, a PI control strategy is adopted.

2.2.1 Heating Module Model

The input of the heating module is the control voltage output from the DAC, and the output is the heating power. Within the normal operating range, the heating power can be approximately considered linearly proportional to the control voltage. The corresponding mathematical model, as shown in Equation (1):

$$P(t)=K_{heat}U(t) \tag{1}$$

where K_{heat}(W/V) denotes the heating gain, representing the change in heating power per unit change in control voltage.

2.2.2 Thermal Dynamics Model of the Controlled Object

The temperature variation of the controlled object (lamp and resonant cavity) is closely related to the absorbed heat. According to basic thermodynamic principles, and neglecting thermal radiation and environmental disturbances, the rate of temperature change is proportional to the input heating power and inversely proportional to the thermal capacitance of the object. Thermodynamic model, as shown in Equation (2):

$$C\frac{dT(t)}{dt}=P(t) \tag{2}$$

where Tdenotes the instantaneous temperature of the controlled object and Crepresents the equivalent thermal capacitance (J/℃). Consequently, the controlled object can be equivalently modeled as an integrator in the control system.

2.2.3 Definition of the Error Signal

The error signal is defined as the difference between the desired temperature and the measured temperature, as shown in Equation (3):

$$e(t)=T_{ref}(t)-T(t) \tag{3}$$

where $T_{ref}$is the desired temperature setpoint and $T(t)$is the measured temperature.

2.2.4 PI Controller Model

A proportional–integral (PI) control algorithm is employed in the temperature servo system. The controller output, as shown in Equation (4):

$$U(t)=K_p e(t)+K_i\int_0^t e(\tau)d\tau \tag{4}$$

where $K_p$and $K_i$are the proportional and integral gains, respectively.

The heated physical system is modeled as an integrator, which, together with the preceding PI controller, forms a temperature servo closed-loop system as shown in Figure 2:

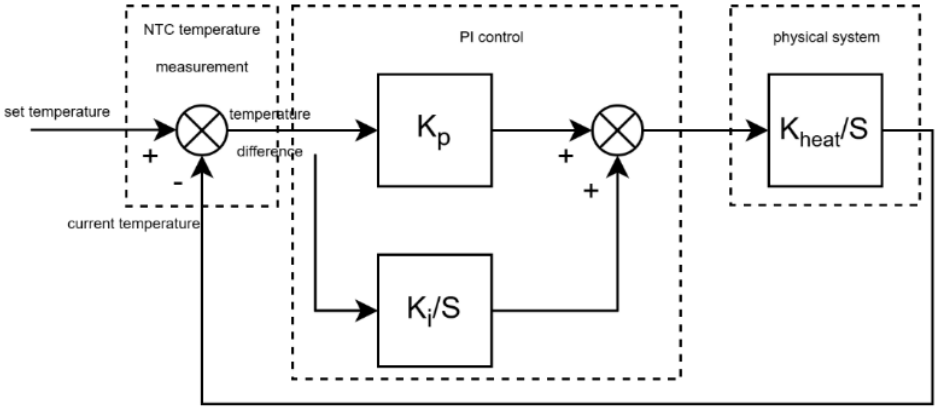

Figure.2 The closed-loop transfer function in the Laplace domain

The closed-loop transfer function of the temperature servo system, as shown in Equation (5):

$$G(s)=\frac{(\mathrm{K}_p+\mathrm{K}_i\frac{1}{s})(\mathrm{K}_{heat}\times\frac{1}{s})}{1+(\mathrm{K}_p+\mathrm{K}_i\frac{1}{s})(\mathrm{K}_{heat}\times\frac{1}{s})}=\frac{\mathrm{K}_i\mathrm{K}_{heat}(s+1)}{s^2+\mathrm{K}_p\mathrm{K}_{heat}s+\mathrm{K}_i\mathrm{K}_{heat}} \tag{5}$$

A standard second-order minimum-phase closed-loop transfer function with a zero, as shown in Equation (6):

$$G(s)=\frac{\omega_n^2(\mathrm{s}+1)}{s^2+2\xi\omega_n s+\omega_n^2} \tag{6}$$

By comparing Equations (5) and (6), the following relationships are obtained, as shown in Equation (7) and (8):

$$\omega_n^2=\mathrm{K}_i\mathrm{K}_{heat} \tag{7}$$

$$2\xi\omega_n=\mathrm{K}_p\mathrm{K}_{heat} \tag{8}$$

where $\omega_n$denotes the undamped natural frequency, $\zeta$is the damping ratio, $K_{\mathrm{heat}}$is the heating gain, and $K_p$and $K_i$are the proportional and integral gains.

The 2% settling time of a second-order system, as shown in Equation (9):

$$\mathrm{t}_s=\frac{4}{\xi\omega_n} \tag{9}$$

From Equations (7) and (9), the controller parameters can be expressed as shown in Equations (10), (11), and (12):

$$\omega_n=\frac{4}{\xi\mathrm{t}_s} \tag{10}$$

$$\mathrm{K}_i=\frac{\omega_n^2}{\mathrm{K}_{heat}} \tag{11}$$

$$K_p = \frac{2\xi\omega_n}{K_{heat}} \tag{12}$$

Substituting Equations (10), (11) and (12) into Equations (4) yields the final PI control law, as shown in Equation (13):

$$U(t) = \frac{8}{K_{heat} t_s} e(t) + \frac{16}{K_{heat} \xi^2 t_s^2} \int_0^t e(\tau) d\tau \tag{13}$$

2.3 Determination of Control Parameters

2.3.1 Heater Gain Calibration

The heater gain K_{heat} characterizes the control voltage-heating power relationship, dependent on heating module characteristics, controlled object thermal capacitance, and heat dissipation conditions. Due to the difficulty in obtaining an accurate theoretical model, an open-loop experimental calibration method is adopted. During calibration, the temperature control system operates in open-loop mode near the thermal equilibrium point; two control voltages V_1 and V_2 are applied, and the corresponding temperature variations ΔT_1 and ΔT_2 are recorded over time intervals Δt_1 and ΔT_2. The temperature change rates are calculated, as shown in Equation (14) and (15):

$$r_1 = \frac{\Delta T_1}{\Delta t_1} \tag{14}$$

$$r_2 = \frac{\Delta T_2}{\Delta t_2} \tag{15}$$

The gain of the heater can be determined as shown in Equation (16):

$$K_{heat} = \frac{r_1 - r_2}{V_{out1} - V_{out2}} \tag{16}$$

This parameter reflects the heating sensitivity of the system under small-signal conditions and serves as a key basis for controller parameter design.

2.3.2 Selection of Second-Order System Parameters

To achieve a reasonable trade-off between response speed and stability, the temperature control system is approximated as a standard second-order system with a damping ratio of $\zeta = 0.707$. Under this condition, the system exhibits fast response with minimal overshoot (approximately 4.3%), satisfying the requirements for temperature control accuracy and stability.

According to the dynamic performance requirements of different components in the rubidium atomic clock, the settling times for lamp temperature and cavity temperature are specified as $t_{s,l}$ and $t_{s,c}$, respectively. The corresponding undamped natural frequencies are calculated using Equation (10).

2.3.3 Calculation of Proportional and Integral Gains

With the determined second-order system parameters and the experimentally calibrated heater gain K_{heat}, the proportional gain K_p and integral gain K_i are calculated using Equations(11) and

(12). This design approach ensures that the closed-loop system meets the desired dynamic performance specifications while maintaining excellent steady-state control accuracy.

2.3.4 Integral Limiting Strategy

The integral term is primarily introduced to eliminate steady-state error. However, if the error persists for an extended period, the integral term may accumulate excessively, causing the control signal to exceed the output range of the DAC, leading to saturation, reduced stability, or even oscillation. Therefore, an integral limiting strategy is necessary[10].

Assuming the maximum DAC output voltage is $V_{\max}$, the maximum allowable integral value is defined ,as shown in Equation (17):

$$\int_0^t e(\tau)d\tau \le \frac{V_{out}(\max)}{K_i} - \frac{K_p}{K_i}e(t) \tag{17}$$

Considering that the error signal magnitude is generally small in practical applications, the integral limit can be approximately set, as shown in Equation (18):

$$\int_0^t e(\tau)d\tau \le \frac{V_{out}(\max)}{K_i} \tag{18}$$

By imposing appropriate upper and lower bounds on the integral term, control signal saturation can be effectively prevented, ensuring linear operation of the system and improving overall stability and reliability.

3. Experimental Results and Analysis

To verify the effectiveness of the proposed PI digital temperature control method based on second-order model parameter calculation, closed-loop temperature control experiments were performed on the lamp and cavity temperature loops of a rubidium atomic clock prototype.

The temperature variation of the lamp and the corresponding output voltage of the lamp PI controller are presented in Figures 3 and 4, respectively. Similarly, the temperature variation of the chamber and the corresponding output voltage of the chamber PI controller are shown in Figures 5 and 6, respectively. The temperature measurement range for the lamp is 108.54 ℃ to 118.01 ℃, while that for the chamber is 72.51 ℃ to 82.56 ℃.

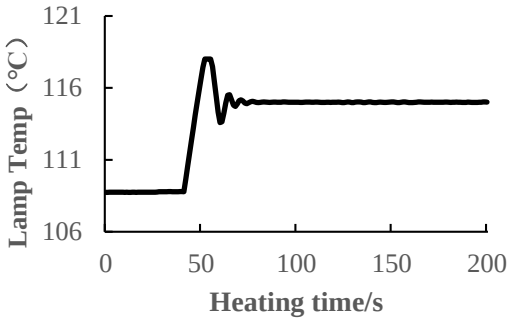

Figure.3 Lamp temperature variation

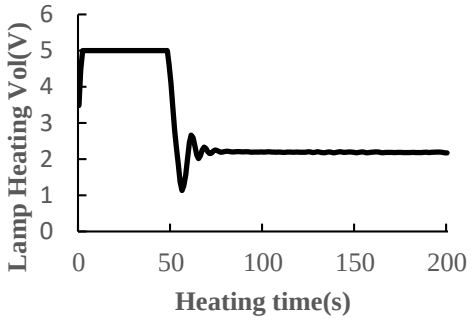

Figure.4 Lamp PI controller output

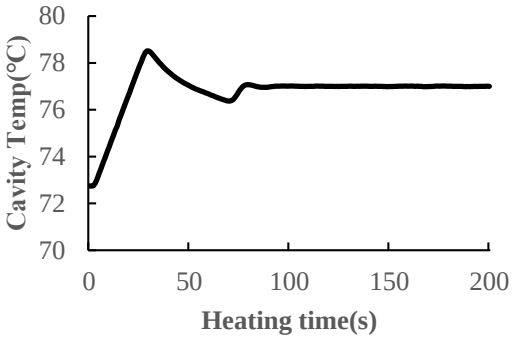

Figure.5 Cavity temperature variation

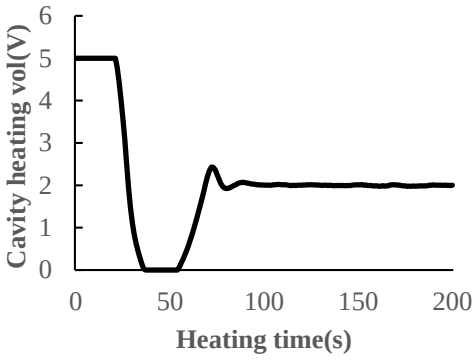

Figure.6 Cavity PI controller output

To ensure the control significance and comparability of the analysis, system performance is evaluated from three aspects: dynamic response, steady-state accuracy, and system stability.

3.1 Dynamic Response Analysis

Experimental curves show that initially, lamp and cavity temperatures are below their measurement lower limits. The PI controller rapidly maximizes output per temperature error, with high heating current driving rapid heating—though measured data barely changes (temperature not entering effective range), showing a "strong actuation–slow apparent temperature variation" phenomenon.

When lamp temperature enters the 108.54 ℃–118.01 ℃ range, measured data accurately reflects its evolution: it rises rapidly to 118.007 ℃, then PI controller output and heating current drop

sharply, transitioning the system from strong actuation to fine regulation and suppressing overshoot.

The cavity temperature loop behaves similarly. Entering the 72.51 ℃–82.56 ℃ range, its temperature rises smoothly toward the setpoint, slower than the lamp due to larger thermal capacitance, but with continuous variation and no oscillation/abrupt changes.

In summary, both loops respond rapidly and transition smoothly from rapid heating to regulated control after entering effective measurement ranges, verifying the proposed PI method's favorable dynamic response performance.

3.2 Steady-State Accuracy Analysis

After 100 sampling points, lamp and cavity temperatures enter steady state. Statistical analysis shows the steady-state average lamp temperature is 115.000 ℃ (standard deviation: 0.012 ℃) and cavity temperature is 77.000 ℃ (standard deviation: 0.0058 ℃), with means close to setpoints and small fluctuations.

Using the 3σ criterion, the steady-state temperature variation is estimated as ±0.037 ℃ (lamp) and ±0.017 °C (cavity). The cavity's smaller fluctuations align with its larger thermal inertia and stronger external disturbance suppression.

In steady state, PI controller outputs for both loops fluctuate narrowly, and heating current mainly compensates for heat dissipation and environmental disturbances. For cavity temperature control, the heating current occasionally drops to zero—when the cavity temperature slightly exceeds the setpoint, the controller promptly cuts heating power to avoid overheating, effectively improving steady-state control accuracy.

3.3 System Stability Analysis

Joint analysis of temperature curves, PI controller outputs, and heating current variations shows that neither the lamp nor cavity temperature control system exhibits sustained oscillation or divergence during startup, heating, regulation, and steady-state operation. Temperature evolution is continuous and smooth, verifying overall closed-loop stability.

For control signals, the PI controller maximizes output during startup for rapid heating, and promptly shifts to fine regulation as temperature approaches the setpoint, with no repeated saturation or abnormal jumps—confirming appropriate PI parameters and sufficient anti-saturation capability.

In steady state, the system compensates for environmental thermal disturbances and internal thermal equilibrium changes via small control adjustments, quickly correcting temperature deviations. This demonstrates the proposed temperature control system's good robustness and disturbance rejection capability[11].

4. Conclusion

This paper proposes a digital temperature control method based on the PI algorithm. A second-order mathematical model is established for the temperature control servo system, where ζ(damping ratio) and t_s(settling time) are quantitatively set, K_{heat} (heater gain) is quantitatively calibrated, and an integral limiting strategy is adopted. Steady-state temperature errors of ±0.04 ℃ for the lamp and ±0.02 ℃ for the cavity are achieved. This method features advantages such as no reliance on parameter tuning experience, flexible adjustment of temperature setpoints, high temperature control stability, and fast response speed. It provides an efficient and reliable solution for temperature regulation of rubidium atomic clocks and offers a reference for other high-precision temperature control applications.

References

[1] Liu K, Guan X, Ren X, Wu J. Disciplining a Rubidium Atomic Clock Based on Adaptive Kalman Filter[J]. Sensors (Basel), 2024, 24(14): 4495.

[2] Guo Y, Wang S, Zhu L, Cai Z, Lu F, Li W, Liu Z. Mitigation of lamp oven and cavity oven temperature-induced frequency variation in rubidium atomic clock[J]. Review of Scientific Instruments, 2023, 94(1): 014706.

[3] Vicarini R, Abdel Hafiz M, Maurice V, Passilly N, Kroemer E, Ribetto L, Gaff V, Gorecki C, Galliou S, Boudot R. Mitigation of Temperature-Induced Light-Shift Effects in Miniaturized Atomic Clocks[J]. IEEE Transactions on Ultrasonics, Ferroelectrics, and Frequency Control, 2019, 66(12): 1962-1967.

[4] Seabra C E D, Dantas T J S, Cavalcanti Y S C, et al. Architecture of an Electrical Equivalence Pyranometer with Temperature Difference Analog Control[J]. Sensors, 2022, 22(21): 8137.

[5] Deepak G, Soumyabrata P, Atharva S, et al. Design and Development of Arduino-Based Four-Channel Data Acquisition System with Digital Temperature Control for Chemiresistive Sensors[J]. Sensing and Imaging, 2024, 25(1).

[6] Gao Y, Zhu W. A Segmented Adaptive PID Temperature Control Method Suitable for Industrial Dispensing System[J]. Electronics, 2025, 14(11): 2306.

[7] Li J, Qin L L, Yue D Z, et al. Experiment Greenhouse Temperature System Modeling and Simulation[J]. Journal of System Simulation, 2008.

[8] He G, Jiang C, Yang M, et al. Research on Cabin Temperature Control of UAV Based on Fuzzy PID Controller[J]. Journal of Innovation and Development, 2025, 10(2): 1-4.

[9] Long K. FDM 3D Printer Temperature Control System Based on PID Control[C]//Proceedings of the 2023 International Conference on Mechatronics and Smart Systems. Lishui: College of Engineering, Lishui University, 2023: 169-176.

[10] Yang C, Ren H, Song Y, et al. Temperature Control Method and Verification for Spaceborne Atomic Clock Based on Phase Change Technology[J]. Journal of Physics: Conference Series, 2024, 2691(1).

[11] Hu E M, Li R Y, Zhang J Y, et al. Design of Digital Temperature Control System for Chip-Scale Atomic Clock[J]. Journal of Astronautic Metrology and Measurement, 2017.